Measuring moonlight: An overview of the spatial properties, lunar coverage, selenolocation, and related Level 1B products of the Moon Mineralogy Mapper

Joseph W. Boardman,[1] C. M. Pieters,[2] R. O. Green,[3] S. R. Lundeen,[3] P. Varanasi,[3] J. Nettles,[2] N. Petro,[4] P. Isaacson,[2] S. Besse,[5] and L. A. Taylor[6]

Received 31 August 2010; revised 31 January 2011; accepted 8 March 2011; published 2 June 2011.

[1] The Moon Mineralogy Mapper (M^3), a high-resolution, high-precision imaging spectrometer, flew on board India's Chandrayaan-1 Mission from October 2008 through August 2009. This paper describes some of the spatial sampling aspects of the instrument, the planned mission, and the mission as flown. We also outline the content and context of the resulting Level 1B spatial products that form part of the M^3 archive. While designed and planned to operate for 2 years in a 100 km lunar orbit, M^3 was able to meet its lunar coverage requirements despite the shortened mission; an increase of the orbit altitude to 200 km; and several relevant problems with spacecraft attitude, timing, and ephemeris. The unexpected spacecraft issues required us to invent a novel two-step approach for selenolocation. Leveraging newly available Lunar Reconnaissance Orbiter-Lunar Orbiter Laser Altimeter (LOLA) topography and an improved spacecraft ephemeris, we have created a method that permits us to bootstrap spacecraft attitude estimates from the image data themselves. This process performs a nonlinear optimization to honor a set of data-derived image-to-image tie points and image-to-LOLA control points. Error analysis of the final results suggests we have converged to a selenolocation result that has image-to-image root-mean-square (RMS) errors less than 200 m and image-to-LOLA RMS errors less than 450 m, despite using data-derived spacecraft attitude results. The Level 1B products include the lunar coordinates resulting from this inversion process and 10 relevant observational geometry parameters that fully characterize the ray tracing geometry on a pixel-by-pixel basis.

Citation: Boardman, J. W., C. M. Pieters, R. O. Green, S. R. Lundeen, P. Varanasi, J. Nettles, N. Petro, P. Isaacson, S. Besse, and L. A. Taylor (2011), Measuring moonlight: An overview of the spatial properties, lunar coverage, selenolocation, and related Level 1B products of the Moon Mineralogy Mapper, *J. Geophys. Res.*, *116*, E00G14, doi:10.1029/2010JE003730.

1. Introduction and Background

[2] The Moon Mineralogy Mapper (M^3) was an imaging spectrometer flown as a guest instrument aboard the Indian Chandrayaan-1 spacecraft. As a NASA Discovery Mission of Opportunity, M^3 was one of several guest instruments on the Indian Space Research Organization's (ISRO) first lunar mission [*Goswami and Annadurai*, 2009]. In a notionally chronological order, this paper discusses the instrument spatial properties, the lunar coverage planned and actually achieved and the selenolocation data processing of the M^3 data. It also provides an overview of the associated products archived in the M^3 Level 1B Planetary Data System archive. M^3 data are archived in three levels: Level 0 (raw data); Level 1B (radiance with supporting selenolocation and geometry) and Level 2 (reflectance), using NASA Data Levels [*Jet Propulsion Laboratory*, 2010]. Our goal is to document and describe the spatial aspects of the instrument, the mission and the observed data and their processing via an optimized pixel-by-pixel ray tracing and the resulting data products. A companion paper [*Green et al.*, 2011] provides more information regarding the instrument design and construction and its spectral and radiometric characteristics and calibration.

[3] The Moon Mineralogy Mapper, as an imaging spectrometer, sought to combine the synoptic view point of orbital imaging with the detailed compositional analysis allowed by high-resolution, high-fidelity reflectance spectroscopy. M^3 was designed to provide data that would allow a global surface compositional mapping of the Moon, as well as detailed and focused examination of high-priority target areas.

[1]Analytical Imaging and Geophysics, LLC, Boulder, Colorado, USA.
[2]Department of Geological Sciences, Brown University, Providence, Rhode Island, USA.
[3]Jet Propulsion Laboratory, Pasadena, California, USA.
[4]NASA Goddard Space Flight Center, Greenbelt, Maryland, USA.
[5]Department of Astronomy, University of Maryland, College Park, Maryland, USA.
[6]Planetary Geosciences Institute, University of Tennessee, Knoxville, Tennessee, USA.

0148-0227/11/2010JE003730

Needing to produce simultaneously high-quality images and high-quality spectra, imaging spectrometers have a series of hurdles to clear before their data can be considered optimally useful and successful. They must balance spectral, radiometric and spatial properties against each other and against realities of hardware capabilities and downlink limitations. Optimal imaging spectrometers must further be stable, uniform, high signal-to-noise and well calibrated. M^3 was designed as a dual-mode imaging spectrometer with these multiple and interrelated challenges in mind. Operating in its Global Mode, with reduced spectral and spatial resolutions, full lunar coverage could be achieved in a single month. The complementary Target Mode, with higher spectral and spatial resolutions was designed for focused study of limited areas of special scientific interest.

[4] The Chandrayaan-1 host spacecraft, built and flown by the Indian Space Research Organization, was designed for a 2 year nominal mission in a 100 km polar lunar orbit. M^3 along with most of the other instruments was mounted on the Anti-Sun-Side panel and aligned for a nadir view of the Moon. Launched from Sriharikota in India on 22 October 2008 the spacecraft was successfully inserted into lunar orbit on 8 November. Shortly after arrival at the Moon it became clear that there were thermal difficulties with the spacecraft caused by its lunar orbit environment. Throughout the mission, the negative effects of these thermal issues forced rapid changes in the nominal mission plan. In May of 2009 the orbit was raised to 200 km to address some of these issues. Contact with the spacecraft was lost prematurely on 29 August 2009 after almost a 10 month mission. Despite the difficulties and shortened mission Chandrayaan-1 was able to collect data with all instruments and to meet the majority of its baseline mission goals [*Green et al.*, 2011].

[5] As is the case for any imaging spectrometer, including M^3, much of the design, performance assessment, calibration, and analysis efforts were focused on the spectral and radiometric aspects. Nevertheless, the spatial characteristics of the instrument, its observations and the resulting data demand commensurate attention. While the well-calibrated spectra can provide a wealth of per pixel compositional knowledge, these results can only be properly reduced and processed and put into a mapping context once the spatial characteristics of the instrument have been accurately quantified. This paper describes the successful result of such a quantification of the M^3 instrument. Despite mission issues and data limitations, we have been able to characterize accurately the instrument's in-flight spatial character and performance, selenolocate the spectrum for each image pixel and derive critical observation geometry parameters.

[6] While the field of photogrammetry, as applied to planetary missions, is mature and well understood, we believe special provisions must be made when dealing with the unique qualities of imaging spectrometry data. Ultimately the radiance spectra are the fundamental building blocks of our M^3 data sets. We consider each observed spectrum as an inviolable unit. Unlike some imaging missions, spatial resampling of the M^3 data would damage the hard-won spectral and radiometric integrity of our measurements by mixing observed spectra. To avoid any such degradation we have archived our Level 1B data with no spatial resampling performed. Instead the spectra that compromise our image cubes are accompanied by accurate and precise selenolocation and observation geometry data on a per pixel basis. In this way the results of the careful measuring of moonlight (reflected sunlight and lunar thermal emission) performed by M^3 are preserved and adequate information is supplied to permit mapping of these measurement and their derived products. This paper provides the background information on M^3, the selenolocation processing, and its Level 1B products, which is needed to map accurately the more than 4 billion lunar spectra measured by M^3 during its 10 months of operation on Chandrayaan-1.

2. Spatial Characteristics of M^3

[7] The Moon Mineralogy Mapper was designed to provide high-fidelity imaging spectroscopy data in two modes of operation: Global Mode and Target Mode. Details of the design are reported in a companion paper [*Green et al.*, 2011]. Here, we focus on its spatial characteristics. As a push-broom imaging spectrometer, M^3 used an area array detector to capture the spatial-spectral image of the light from an entrance slit, after it was dispersed by a grating element. The design was optimized to create uniform and stable data with high signal-to-noise properties [*Mouroulis et al.*, 2000]. The nominal field of view was 24°, giving approximately a 42.5 km swath from a 100 km orbit. The detector array is a 640 sample by 480 line HgCdTe TMC 6604A detector from Teledyne. The portion of the focal plane illuminated by the spectrally dispersed slit image spans 608 detector samples in the spatial direction and 260 detector lines in the spectral direction. The instantaneous field of view of a single cross-track column of the array was approximately 700 microradians, giving a surface pixel size of 70 m from the nominal 100 km orbit.

[8] High-resolution Target Mode data are created by recording the data, detector by detector, as measured by the focal plane, creating images with 608 illuminated cross-track samples and 260 spectral bands. The lower-resolution Global Mode data are created from the raw observed data in the M^3 onboard computer by coadding two frames from the detector and binning by a factor of two in the spatial direction and by factors of two or four in the spectral direction. Selected spectral regions near diagnostic absorption regions were binned by a factor of two in order to retain higher spectral resolution. The resulting Global Mode data have 304 cross-track samples and 86 spectral bands. The nominal Global Mode pixel size is 140 m, double the Target Mode pixel size. The first band of the 86 Global bands created on board is not included in the Level 1B archive, due to low signal fidelity. With the combined spatial and spectral binning, Global Mode data have a factor of 12 reduction of data rate as compared for full-resolution Target Mode data (four times reduction in pixel count and approximately three times reduction in spectral band count). Global Mode was optimized to allow continuous lunar coverage yet still meet the downlink constraints of the Chandrayaan-1 mission. Target Mode was designed to optimize spatial and spectral information content for specific areas of high interest.

[9] The entrance slit of M^3 has a curved projection in object space, as a consequence of the strict requirements to have a uniform and rectilinear spatial-spectral photon dispersion pattern on the detector array. Instead of allowing this

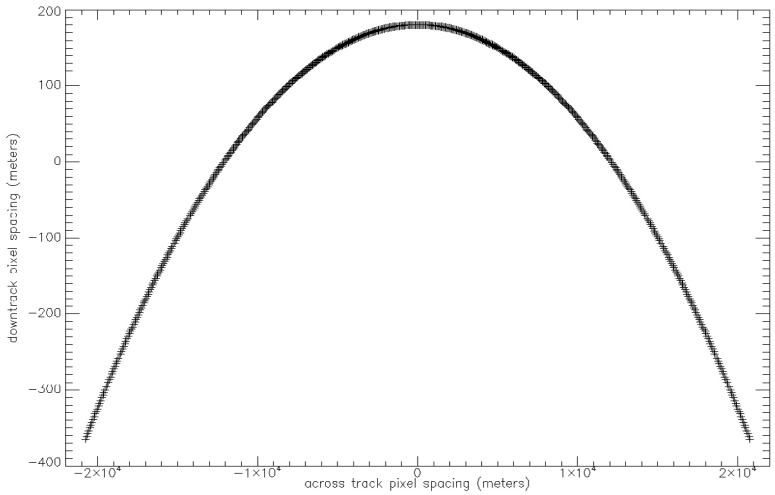

Figure 1. Preflight characterization of the curved slit projection in object space, showing the nominal pixel-center spacings after projection onto a horizontal surface from an elevation of 100 km.

curvature to occur inside the instrument, where it introduces spectral "smile," differences in spectral response per band across the detector array, and the associated nonuniformity in the data, M^3 essentially put the "smile" outside the instrument in the projected image of the slit on the surface of the Moon. Figure 1 shows the preflight characterization of the slit projection curvature. This amounts to approximately 600 m of downtrack curvature across the nominal 24° and 42.5 km swath, or 1.4%. Depending on whether the Chandrayaan-1 spacecraft was flying forward (zero yaw) or backward (180° yaw), this slight bow in the projected slit either leads or follows the nadir location. While this curvature, or "spatial smile," does introduce a slight systematic distortion to the raw Level 0 and Level 1B images, it is much better than having the equivalent "spectral smile" on the focal plane causing spectral/spatial nonuniformity resulting in data of compromised quality. Panoramic distortion and lunar topography already introduce irregularities in the surface grid of observed pixel centers. Extra distortion due to the slit projection curvature can be easily compensated, and its effects are fully included in our camera modeling and optimized selenolocation and ray tracing. In section 5, we report the derived inflight camera curvature model that resulted from a joint inversion of the observed data.

[10] The M^3 system was designed so that photons collected for all bands of a single spectrum came from the same local pixel area on the lunar surface. This requirement is critical, so that the observed spectra are meaningful and realistic. As with "smile," this requirement leads to a design that provides a well-aligned rectilinear spatial/spectral dispersion pattern on the array, avoiding "keystone," "twist" and "IFOV shift." These aspects of the design are discussed in the companion paper [*Green et al.*, 2011]. Characterization of the across-track spatial response of M^3 was conducted by laboratory measurements during preflight calibration. These laboratory calibration data are available in the M^3 PDS archive. All data produced by M^3 met its strict uniformity requirements. The slight asymmetry of the response functions is a result of design tradeoffs involving the readout timing and noise sources.

[11] The downtrack response of the M^3 system is governed by the timing of the readout and the projected angle of the entrance slit. The slit was designed to have the same 700 microradian angle as the cross-track detector columns. This static response is then integrated downtrack through time for the duration of the instrument integration time. The nominal M^3 Target Mode integration time was 50 ms, giving approximately twenty Target Mode frames per second. Global Mode, combining two Target Mode frames, has approximately a 10 Hz effective frame rate. At the nominal 100 km altitude the Chandrayaan-1 spacecraft had a downtrack velocity of approximately 1400 m/s. The resulting M^3 pixel center spacings were thus designed to be nearly equidistant in the cross-track and downtrack direction: 70 m for Target Mode and 140 m for Global Mode. M^3 was designed to have overlapping swaths in adjacent orbit tracks. In the overlap areas M^3 could potentially be used to develop stereo models to derive lunar topography. Stereo use of M^3 data has not been addressed by this study.

3. Nominal Coverage Plan

[12] The original M^3 mapping plan for lunar coverage was based on the expected 2 year Chandrayaan-1 nominal mission. During that 2 year mission, M^3 planned to operate during four optical periods. Each optical period was defined as an approximately 3 month time span, when the solar zenith angle at the lit-side equatorial node of the orbit was less than 45°. The 2 month central section in each optical period, where the solar angle to the orbit plane (beta angle) was less than 30°, was expected to be the prime M^3 observation time span. This period, centered on the zero-beta noon-midnight orbit phase, provided maximum reflected signal and minimal cast shadows. Supplemental imaging was planned for the 30° to 45° beta angle "wing periods" on each side of each optical period. Figure 2 shows a schematic illustration of the orbit and illumination geometry for a single year, illustrating two optical periods 6 months apart.

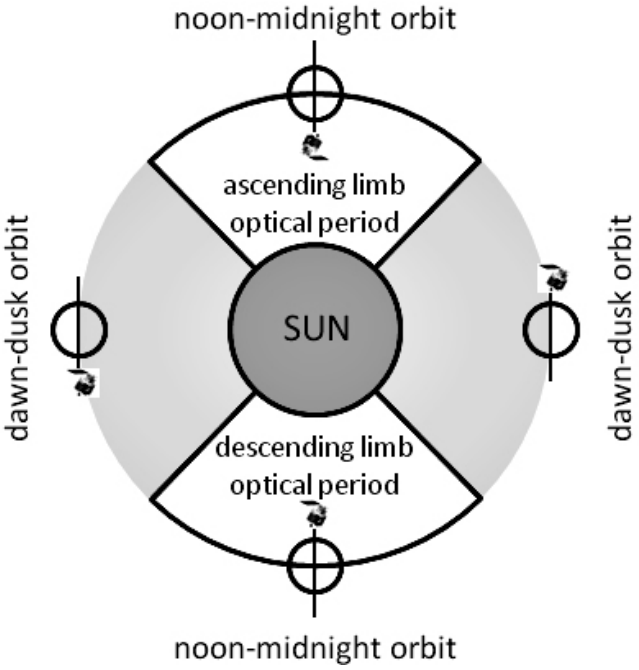

Figure 2. Schematic diagram showing the inertial Chandrayaan-1 orbit around the Moon and the changing illumination angle during a year of operations. Two 3 month optical periods were planned in each year, 6 months apart, centered on the noon-midnight orbit orientation. The full mission was to be 2 years and four optical periods.

[13] During the first month of continuous operations in the first optical period M^3 operations were planned to provide complete lunar coverage in the reduced-resolution Global mode (140 m pixel spacing and 85 spectral bands). This was to be accomplished in a single sidereal month via 334 Global Mode imaging events, one per each 118 min orbit, each spanning approximately 48 min duration and 145° of latitude. We allowed for the expected orbital height variations (80 km to 120 km, with a 100 km nominal value) and the expected extremes of lunar topography of >±9 km relief relative to the reference radius of 1737.4 km [*Archinal et al.*, 2006] (subsequently refined to −9.1 km and +10.7 km, [*Smith et al.*, 2010]), leading to an optimized coverage strategy employing alternating swaths of 145° latitude extent. These alternating swaths, on an odd-even pattern, would start at the North Pole and extend to 55°S latitude, then start at 55°N latitude and extend to the South Pole. Figure 3 shows the layout of the nominal pattern with odd and even orbit number swaths indicated. Poleward of 55° latitude, alternate image swaths are adequate for full coverage, with the same overlap that adjacent orbit swaths have at the equator, even accounting for orbit and topographic effects. Each orbital swath is also preceded by a dark image collection of 20 s of data taken at 80° latitude on the dark side of the Moon, before crossing to the lit limb of the orbit.

[14] The prelaunch plan stated that once the complete Global Mode coverage was accomplished, during Optical Period 1, M^3 would switch over to almost exclusively perform data acquisitions in its high-resolution (70 m pixel center spacing and 260 spectral bands) Target Mode. A global set of low-, medium- and high-priority science targets were developed for this portion of the mission. Figure 4 shows the proposed premission target database. It was expected that given the downlink-constrained nature of the Chandrayaan-1 mission, we could expect to achieve up to 25% coverage of the Moon in Target Mode. It was also planned that Target Mode locations would be added to the target list based on preliminary analysis of Global Mode data sets.

[15] As with nearly all space missions, unexpected conditions forced the Chandrayaan-1 and M^3 teams to redesign the mission in real time. This was necessary to fit the rapidly evolving situations that threatened the survival of the spacecraft, affected the instrument and limited the imaging and downlink opportunities. The M^3 Team is forever grateful to the Chandrayaan-1 Mission Operations team for their work in flexibly replanning the mission throughout its duration; these efforts assured that M^3 could meet its baseline mission requirements despite the numerous unexpected challenges. Section 4 describes the actual M^3 coverage his-

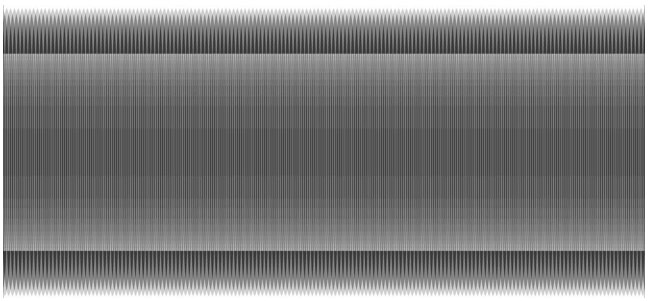

Figure 3. Swath layout for Global Mode full lunar coverage. The 145° latitude swaths alternating on an odd/even pattern provide complete coverage, despite orbit variations and topographic effects. Areas of single coverage through four times or greater coverages are shaded as a gray scale. The alternating sets of odd/even orbits are seen in the bands at 55°S and 55°N latitude. The full Moon in a simple cylindrical projection is shown.

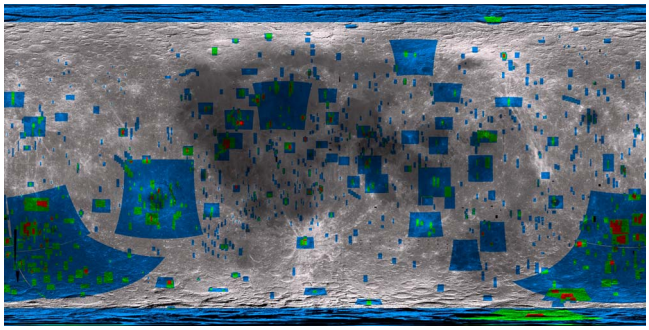

Figure 4. Premission Target Mode database. High-, medium-, and low-priority targets are shown in red, green, and blue overlays, respectively, on a Clementine-ULCN base map [*Hare et al.*, 2008] in a full Moon simple cylindrical projection.

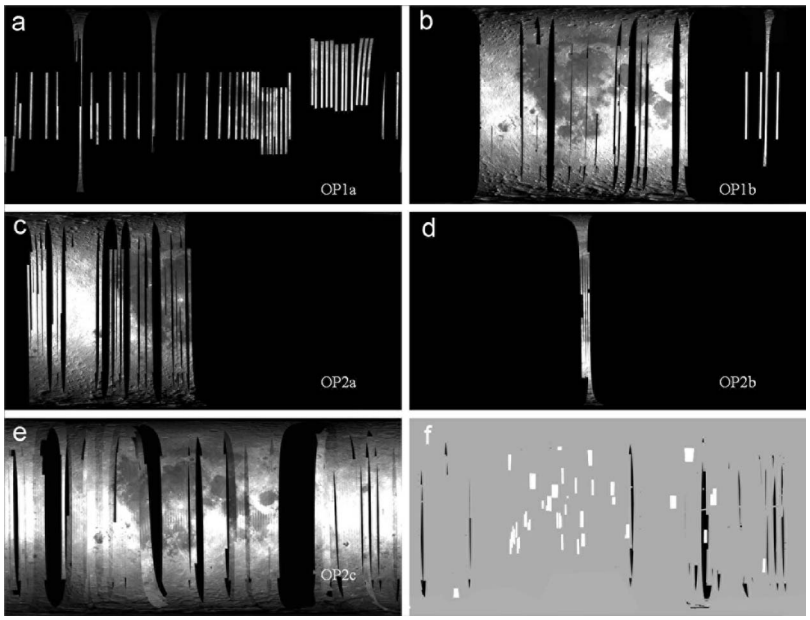

Figure 5. (a-e) Summary image mosaics of M^3 coverage by suboptical period. (f) The summary image shows composite Global Mode coverage in gray, the limited Target Mode images in white, and the few mission gaps in black. Each image is a full Moon simple cylindrical projection, centered at zero longitude.

tory that was accomplished during the abbreviated 10 month Chandrayaan-1 mission.

4. Actual Coverage History

[16] The Chandrayaan-1 mission was beset by thermal issues on the spacecraft from the time of arrival at the Moon on 8 November 2008. Before any images were taken, the spacecraft lost one of its redundant Bus Management Units and one of its two star trackers. ISRO immediately began replanning the mission to ensure the spacecraft survival and to rebalance operational and observational requirements. An extended commissioning phase that lasted through January 2009 involved M^3 collecting periodic abbreviated images on a few orbits per day, instead of the planned 48 min images on each of twelve orbits per day. M^3 was later operated in its full coverage Global Mode for several discrete periods within the mission, starting initially on 31 January 2009. Because of the thermal issues, the imaging times were moved to periods of higher beta angle, increasing phase, reducing the reflected signal and increasing the effect of surface shadows in the data. The second optical period began 15 April 2009 with M^3 in full operation. However, by mid-May, the second star tracker was lost, and ISRO decided to raise the orbit to 200 km, due to limited attitude knowledge. The original 100 km orbit required frequent orbit adjustment maneuvers, which themselves required detailed attitude knowledge. After the orbit was raised, M^3 was again operated mostly in Global Mode to complete our baseline lunar coverage, with a limited number of Target Mode observations. The last M^3 images were collected on 16 August 2009 as the increasing solar beta angle ended Optical Period 2. Contact with spacecraft was lost unexpectedly on 29 August 2009, after nearly 10 months in lunar polar orbit.

[17] Despite the significant unexpected challenges of the abbreviated mission, M^3 was able to exceed its mission requirements in Global Mode of nearly complete (more than 90%) lunar coverage, but was only able to collect a minimal number of Target Mode scenes. M^3 was operated, often at a reduced duty cycle, during only two optical periods instead of the planned four. Further, the imaging periods were extended into times of higher solar zenith angle than originally planned. As a result of the number of operational variations during the mission, the two optical periods were informally subdivided into segments based on the altitude and spacecraft status. Table 1 details the dates, operational situation and image collections achieved in each of the observation periods. Figure 5 illustrates the associated lunar coverages accomplished in each optical period, along with a summary image showing our cumulative coverage in both Global and Target Modes, in a simple cylindrical projection of the full Moon, centered on zero longitude. Figure 6 shows combined summary coverage images for both North and South Pole regions, poleward of ±60° latitude, in a polar stereographic projection.

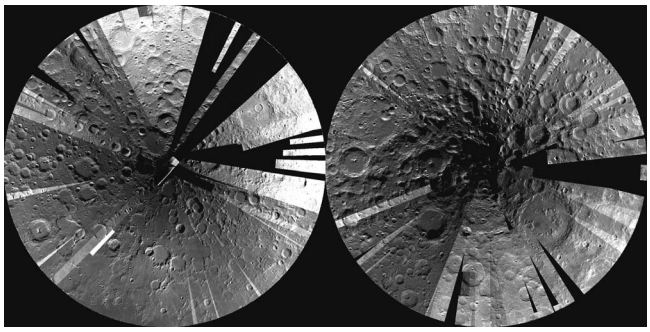

Figure 6. (left) North and (right) South Pole full-mission summary coverages in polar stereographic projections for the areas poleward of ±60° latitude.

Table 1. Optical Period and Coverage Summary

Period	Dates	Images	Orbit	Star Sensors	Status
OP1A	Nov 18–Jan 24	119	100 km	1 of 2	extended commissioning
OP1B	Jan 25–Feb 14	247	100 km	1 of 2	operational, high solar zenith angles
OP2A	Apr 15–Apr 27	197	100 km	1 of 2	operational, high solar zenith angles
OP2B	May 13–May 16	20	200 km	0 of 2	S/C emergency, orbit raised
OP2C	May 20–Aug 16	375	200 km	0 of 2	operational, variable conditions

[18] After the orbit was raised to 200 km, the spatial sampling and resolution of the M^3 data were obviously altered. The downtrack pixel center spacing was only slightly increased, from 140 m to 153 m, due to the slightly longer period orbit at the higher altitude. M^3 had a fixed frame rate and operated identically in the higher-altitude orbit. Conversely the across-track pixel center spacing and swath width doubled in the higher-altitude orbit. The doubled swath width allowed for a 50% duty cycle to achieve full coverage, imaging on every other orbit. Nearly the full Moon was covered from this higher orbit.

5. Selenolocation Methodology and Data Processing

[19] Accurate ray tracing to derive pixel center locations relies on a number of equally critical inputs. These include spacecraft ephemeris (position and velocity), spacecraft attitude (pointing), image frame timing, geometric camera model and details of the observed body, including its position, rotation and topographic model, in a well-defined reference frame. Our approach was to develop and apply a physical model for the M^3 observation, including all of the above parameters. We also included the less important, but measurable, effects of one-way light time-of-flight and spacecraft velocity aberration of the look directions. Our initial goal was to provide selenolocations and associated observation geometry on a per pixel basis with a desired root-mean-square (RMS) error on the order of the pixel size. The error budget of the final accuracy can be tracked directly to the four major auxiliary inputs: timing, ephemeris, attitude and topography. For a nominal one pixel error in Global Mode, from the 100 km orbit, the respective errors required in each of these four independent parameters are 100 ms timing, 140 m ephemeris position, 1400 microradians of pointing error and more than 658 m of vertical topographic error.

[20] A number of issues with the initially available auxiliary data and the Chandrayaan-1 mission complicated that effort. Using the timing, attitude and ephemeris data, as supplied, gave us unacceptably large location errors, up to tens of kilometers, both between overlapping M^3 images and between M^3 images and all available selenodetic controls. These errors, when examined from a global perspective seemed to have multiple, yet unknown, underlying causes. The errors were often locally systematic, yet wildly variable through time and across the Moon. No amount of adjusting expected camera or bias parameters could achieve an adequate solution. As a result, we were forced to redesign our selenolocation methodology and use the M^3 data themselves to bootstrap a consistent and low-error solution, leveraging newly available inputs from a variety of sources to tie the M^3 data to a lunar frame. With the redesigned selenolocation scheme, we have met our goals and the data produce nearly seamless mosaics and tie to the absolute reference frame at a RMS error level of several pixels. This bootstrapped result represents an improvement in accuracy and precision of nearly two orders of magnitude over our initial attempts.

[21] The processing methodology for the selenolocation of the M^3 data involves a pixel-by-pixel ray tracing performed in a two-tiered approach, illustrated in Figure 7. First, we perform an initial ray tracing using the ephemeris, attitude, timing and camera model data, as provided by ISRO and JPL. Second using the results from this initial ray tracing, we developed a network of image-to-image tie points and image-to-absolute location control points. This control network was used as an input to a global optimization of attitude and camera model parameters. A second ray tracing was performed using the optimized camera model and the control network-derived attitude parameters. This second, optimized, ray tracing creates the spatial products delivered as part of the M^3 Level 1B PDS archive. The following text discusses the development of the inputs to this two-tiered

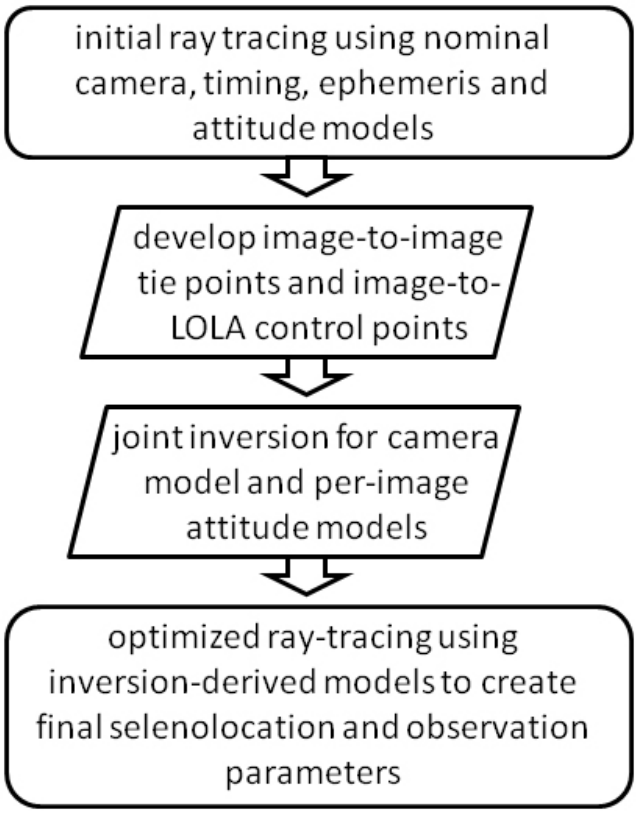

Figure 7. Schematic flowchart depiction of our two-stage bootstrapping selenolocation methodology.

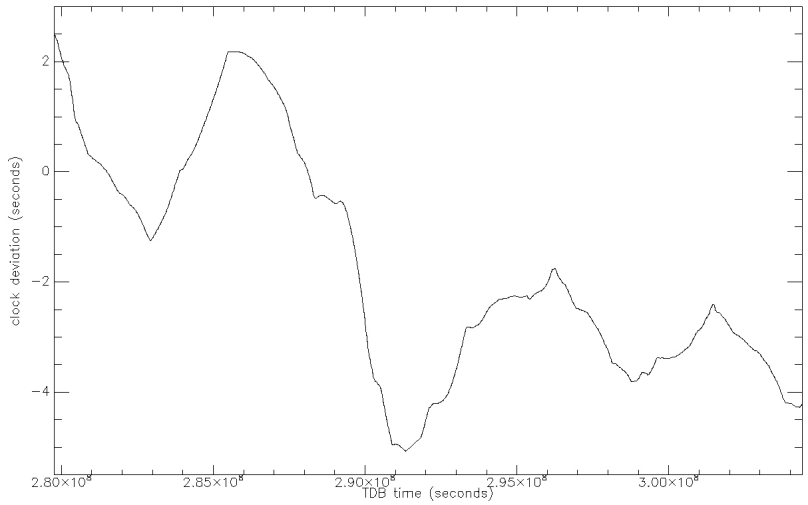

Figure 8. Deviation of our model of the Chandrayaan-1 clock from a perfect-rate, no-drift clock, based on a TDB epoch of J2000.0.

bootstrapping methodology and gives examples of the various outputs.

[22] Timing is obviously critical for accurate ray tracing and pixel center location. M^3 and Chandrayaan-1 each had free running clocks that counted raw ticks rather than absolute time. The Chandrayaan-1 clock had a nominal tick rate of 1000 Hz while the M^3 clock ran at 12 MHz. The Chandrayaan-1 clock rolled over after 21 days so its values are bound in the range 0 to 1,814,399,999. Each rollover started a new Chandrayaan-1 clock partition. The M^3 clock did not roll over during the mission. Within the Level 0 M^3 data each image frame is tagged with the M^3 clock tick count. Additionally, once per minute, the simultaneously valid M^3 and Chandrayaan-1 time ticks are recorded in frame headers of the M^3 Level 0 data. Using these time tick pairs we developed a per scene regression that related M^3 ticks to Chandrayaan-1 ticks. To aid in tying Chandrayaan-1 ticks to Barycentric Dynamical Time (TDB) ISRO provided raw telemetry data that link Chandrayaan-1 ticks and Earth-station-received times. We processed these data to remove the effects of Earth and Moon location and rotation, one-way travel time and buffering bias and removed spurious and anomalous points. Using these processed data we were able to build a clock kernel [*Acton*, 1996] that relates onboard Chandrayaan-1 ticks to Barycentric Dynamical Time (TDB). The resulting piecewise linear clock model required 504 segments to track the observed data to a tolerance of ±2 ms. This clock kernel is a part of the M^3 PDS Level 1B archive. Figure 8 shows the deviation of the onboard clock to a no-drift, perfect-rate clock. ISRO periodically reset the onboard clock rate to keep the deviation bounded within approximately three seconds of nominal. The original clock data, as provided, ignored the deviations from nominal and admitted timing errors of up to several seconds and contributed to selenolocation errors up to five kilometers.

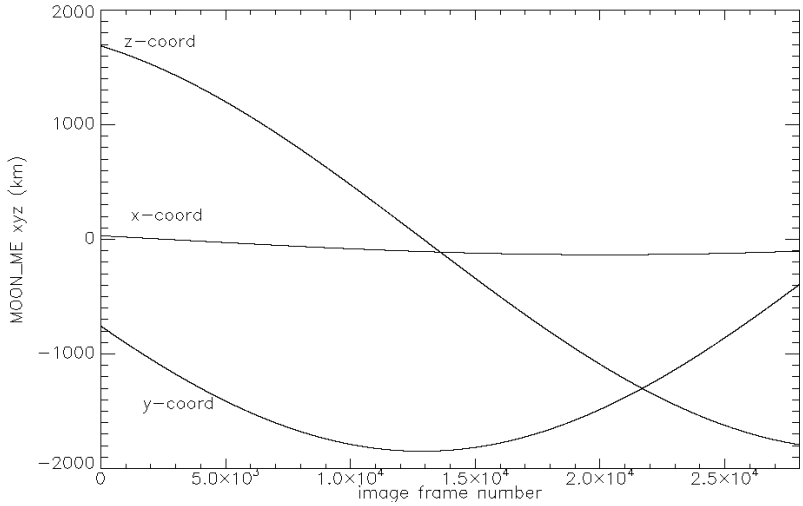

Figure 9. Typical Chandrayaan-1 ephemeris data for a single descending limb image, as expressed in the MOON_ME rotating reference frame.

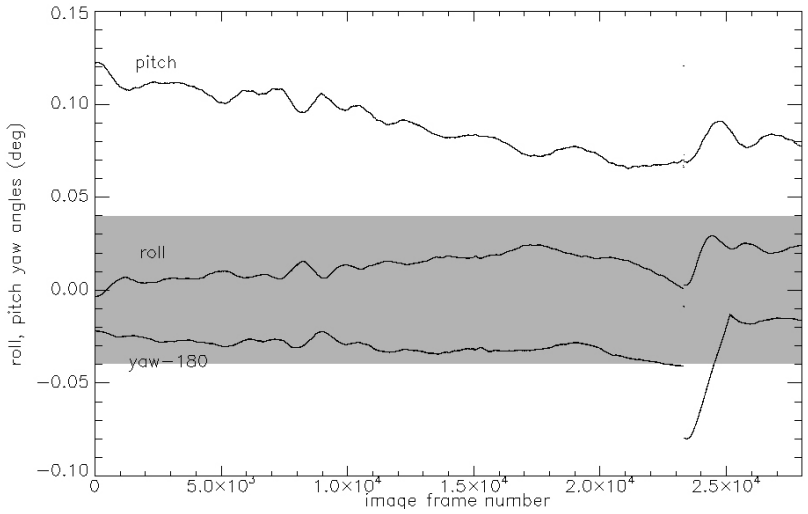

Figure 10. Typical spacecraft-reported roll, pitch, and yaw data for a single image, relative to an ephemeris-defined instantaneous nadir looking orbital frame. The yaw value has had 180° subtracted to be plotted on the same scale, as this was a reversed-flight time period. The gray band centered on zero shows the equivalent angular width of a single Global Mode pixel field of view (1400 microradians or 0.08°).

[23] We used ephemeris data from two different sources in our processing. During the mission, we were provided with ongoing, rolling 21 day SPK [*Acton*, 1996] ephemeris kernel files from ISRO that described two days of derived ephemeris appended with 19 days of predicted data. We used these during the mission for our initial ray tracing efforts. In late March 2010 we were supplied a separate full-mission SPK ephemeris data file from JPL. Chandraayan-1 data were downlinked to stations in India, Maryland and California. JPL developed an independent ephemeris using the ranging data from the two United States stations. We used this JPL-developed ephemeris for all of our final processing and selenolocation solutions, and the associated SPK kernel is included in the M^3 PDS archive. A direct comparison of the two ephemeris data sets shows time varying, but locally systematic, differences of up to tens of kilometers. The JPL solution has expected errors of less than 150 m, on the order of or smaller than the M^3 pixel size (N. Mottinger, personal communication, 2010). Ephemeris data for a typical orbit are shown in Figure 9. The location and orientation of the Moon were developed from the DE421 ephemeris (de421.bsp) and the associated planetary rotation frames (moon_pa_de421_1900–2050.bpc) [*Folkner et al.*, 2008].

[24] Spacecraft attitude data were supplied by ISRO both during the mission and in a summary fashion after the conclusion of operations. We determined that we were unable to solve for a stable camera model that honored scene-to-scene overlaps and that tied to the absolute lunar reference frame using these data as delivered. No doubt the loss of the first star tracker before imaging operations began and the loss of the second star tracker in the second optical period limited the available attitude knowledge information and its accuracy. Instead of using the attitude data in an absolute form, we use them in a relative fashion to assess the temporal stability of the spacecraft during imaging periods. We suspect the attitude data may be inaccurate in an absolute reference frame sense yet preserve a useful depiction of the relative temporal rotation of the spacecraft within single image collections. For Optical Period 1 we see that the spacecraft attitude, relative to an ephemeris-defined orbit frame (nadir +Z, right-side orbit normal +Y and frame completing vector that is nearly parallel with velocity +X) is stable in pointing to better than one M^3 Global Mode pixel (approximately 1400 microradians). Given this temporal stability, for the mission period in the 100 km orbit, we have been able to bootstrap per scene attitude profiles using the control points and tie points generated in the second phase of our two-step selenolocation processing. Figure 10 shows the roll, pitch and yaw relative to the instantaneous orbital frame, as indicated by the ISRO data, for a typical orbit. Also shown is the relative angular size of one M^3 pixel. Processing of Optical Period 2 data is ongoing at the time of this writing, and the latter portion of this period is proving more challenging. At the 200 km orbit, with no star trackers, the spacecraft was less able to maintain the desired nadir attitude. For these data, we are applying an extended attitude derivation model in which we solve for an initial attitude bias at the dark limb node crossing time and an arbitrary axis of rotation in J2000 along with an angular rate about that derived axis. We are achieving similar RMS errors using this model as produced by the simpler model in the earlier data Optical Period 1 data when the spacecraft was more stable. All of our derived attitude parameters and associated models are included in our PDS Level 1B archive. Despite the limitations on available attitude data we believe our selenolocation method sidesteps this critical deficiency and uses the data themselves along with auxiliary topographic data to bootstrap adequate per orbit attitude models.

[25] Our initial source for topographic data was the Unified Lunar Control Network (ULCN) 2005 [*Archinal et al.*, 2006], as it was the best available data set at the beginning of our mission. Fortunately we have been able to shift to the excellent new lunar topography developed by the Lunar

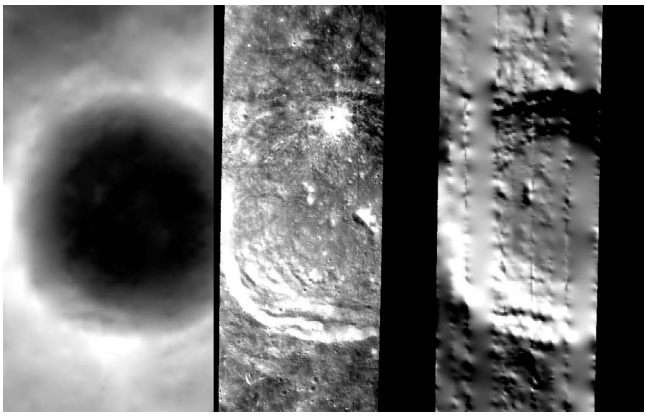

Figure 11. Example of LOLA gridded topography, associated M^3 Band 20 imagery and a shaded relief of the LOLA topography using solar angles corresponding to the M^3 collection times. Artifacts due to incomplete LOLA coverage at the time of our usage, and the resulting banding from interpolation, are obvious at the right-hand side.

Orbiter Laser Altimeter (LOLA) [*Smith et al.*, 2010]. While the ULCN data were relatively sparse with typical point-to-point separations of ten kilometers or more, the LOLA data, at least in polar regions, exceed the sampling density of the M^3 pixels [*Smith et al.*, 2010]. While the initial LOLA data became available at an opportune time, shortly after termination of Chandrayaan-1, the Lunar Reconnaissance Orbiter mission is not yet complete at the time of this writing and our first PDS delivery. As such, the LOLA topographic model is still incomplete, especially in low-latitude areas where the across-track coverage continues to be filled in. Further, as we used LOLA data during their ongoing mission, their final crossover adjustment and refinements had not been included. Figure 11 shows a typical LOLA subset and matching M^3 imagery, along with a simulated shaded relief image of the LOLA digital elevation model. Despite their limitations and incomplete nature at the time we had to use them, the initial LOLA data play a key role in our bootstrapping method allowing us to lock the M^3 mosaic onto an absolute selenodetic frame. Although not currently funded, we look forward to an eventual reselenolocation of the entire M^3 data set onto an improved topographic product, incorporating the new altimetry and stereo data that will soon be released. Eventually we hope to use an optimized and merged lunar topographic model, with global topography at the near-pixel scale for M^3, combining LOLA and Kaguya altimetry [*Araki et al.*, 2009] with the stereo models being developed from Lunar Reconnaissance Orbiter Wide-Angle Camera data [*Robinson et al.*, 2010] and the Terrain Camera on Kaguya [*Haruyama et al.*, 2009].

[26] Our bootstrapping inversion method relies on a network of data-derived tie points and control points to solve for the M^3 camera model and the per orbit attitude history of the Chandrayaan-1 spacecraft. We utilize a modified version of the Scale Invariant Feature Transform image matching technique [*Lowe*, 2004] to generate both our tie points and our control points. SIFT is very robust and easily establishes many valid tie points between adjacent-orbit M^3 scenes in their areas of overlap. To facilitate this process we find the area of overlap, using nominal attitude parameters, and render both scenes into the common map projection and grid of a locally relevant Transverse Mercator projection. Then, tie points are created and related back to the raw sample and line numbers from the two input images. Figure 12 shows a typical subset of tie points generated in a pair of adjacent-orbit images orthorectified into a common projection covering the overlap area. These M^3 image to M^3 image tie points drive the inversion to a solution that demands seamless image overlaps. The link between the M^3 data and the absolute lunar reference frame is created by a similarly generated set of control points. The control points tie M^3 orthorectified images to similarly projected LOLA topography images, asserting the LOLA selenolocations as a virtual lunar control network. To aid the image matching we render a simulated scene using the LOLA topography and the solar azimuth and zenith angles that correspond to the M^3 image frame times. While SIFT is a powerful image matching method, it often struggles with the M^3 to LOLA matching and the control points generated must be carefully weeded of spurious outliers. In cases of low solar zenith angles, with few or no shadows and subdued topographic effects, the method often fails completely and control points are picked by hand. However, in many scenes, especially those with high solar zenith angles, adequate control points are automatically generated and vetted. The M^3 to LOLA matching is further hindered by the incomplete nature and variable sampling of the midmission LOLA data we used. At lower latitudes the LOLA data are sparser, with typical intertrace gaps of several kilometers. The interpolation to give a continuous data set limits the accuracy of the M^3 to

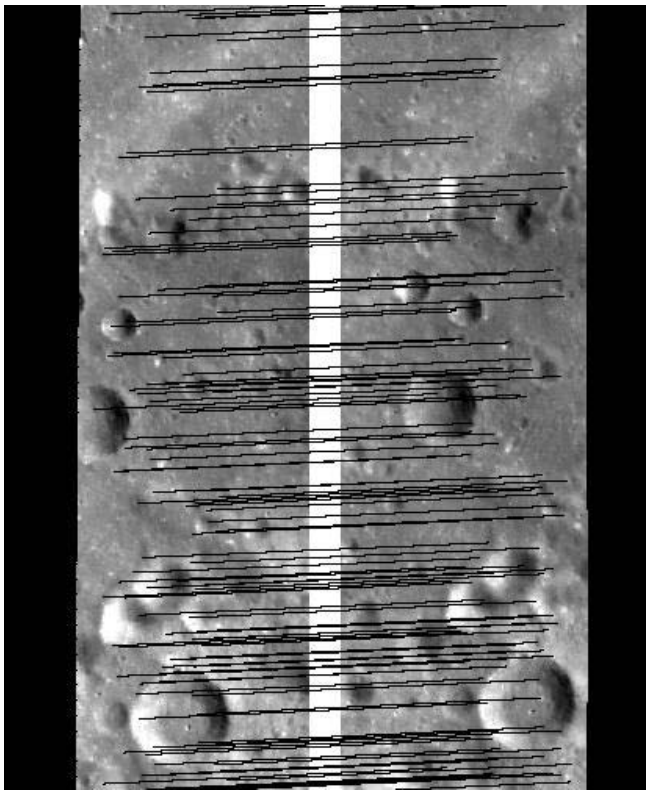

Figure 12. Example of automatic tie points generated for inversion model, using the common area in two overlapping M^3 images strips from adjacent orbits.

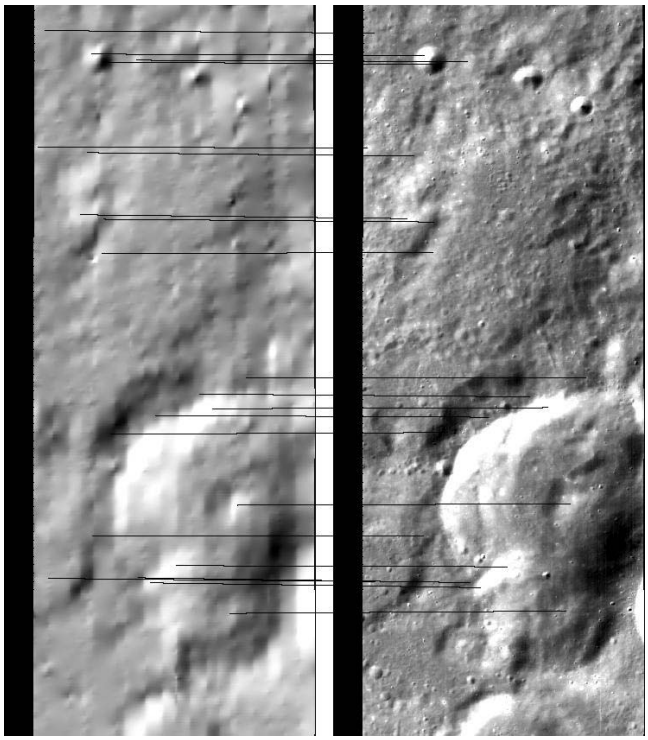

Figure 13. Example of automatic control points for inversion model, using M^3 imagery and a shaded relief built using LOLA topography illuminated at the same solar angles as the M^3 overpass. Comparing Figures 12 and 13 reveals the increased level of difficulty in control point creation relative to tie point creation.

LOLA matching as a function of latitude. This is in contrast to the much easier M^3 to M^3 image matching to develop tie points. We believe this inherent accuracy and precision difference explains much of the observed error differences in the final fits of the tie points and control points, as discussed below. Figure 13 shows a typical M^3 scene subset and the illuminated LOLA model, along with the automatically generated control points.

[27] Armed with accurate ephemeris, timing, and topographic data augmented by a dense network of image-to-image tie points and image-to-reference frame control points; we can now formulate an inversion problem to solve for a parameterization of the in-flight camera model and per orbit attitude profile parameters. We employ a Levenberg-Marquart nonlinear inversion process [*Levenberg*, 1944; *Marquardt*, 1963] to estimate the optimization parameters, so as to minimize the total error in the model. The total error is measured as the RMS of the tie point and control point mismatch distances. For the Optical Period 1 data, we solved for a single set of roll, pitch and yaw angles for each orbit, measured with respect to an ephemeris-derived, perfect-nadir instantaneous orbit frame, and four camera parameters that define the field of view and curvature of the projected slit image. The nonlinear optimization adjusts the free parameters of the spacecraft attitudes and the camera model so as to align all of the control points with the lunar reference frame and to align all of the tie points so there is no scene-to-scene mismatch. The Optical Period 1 inversion solved for 490 total attitude and camera parameters using a combined 57,929 ground control and tie points. Figure 14 shows before and after inversion error plots, where the before plots use a nominal nadir attitude estimate and the lab-measure camera model. In each plot of Figure 14 the first 28,907 points are the control points and the last 29,022 points are the tie points. In the case of the control points, error is measured as the distance from the ray traced pixel center to the reference location as identified in the illuminated LOLA image. In the case of the tie points the error is measured as the distance between the ray traced pixel centers for each half of the tie point pair. The RMS error for the control points is reduced from 1696.4 m to 414.3 m. For the tie points the RMS error is reduced from 462.8 m to 180.9 m. As expected the tie points converge better than the control points as they are higher-quality matches of very similar imagery. Figure 15 shows a scatterplot of the horizontal x and y map difference of the control point errors, showing the zero-mean and randomized result. We suspect that the true deviation of our alignment to the absolute frame is on the order of the smaller tie point error, but cannot independently prove it as we use the LOLA data both as a

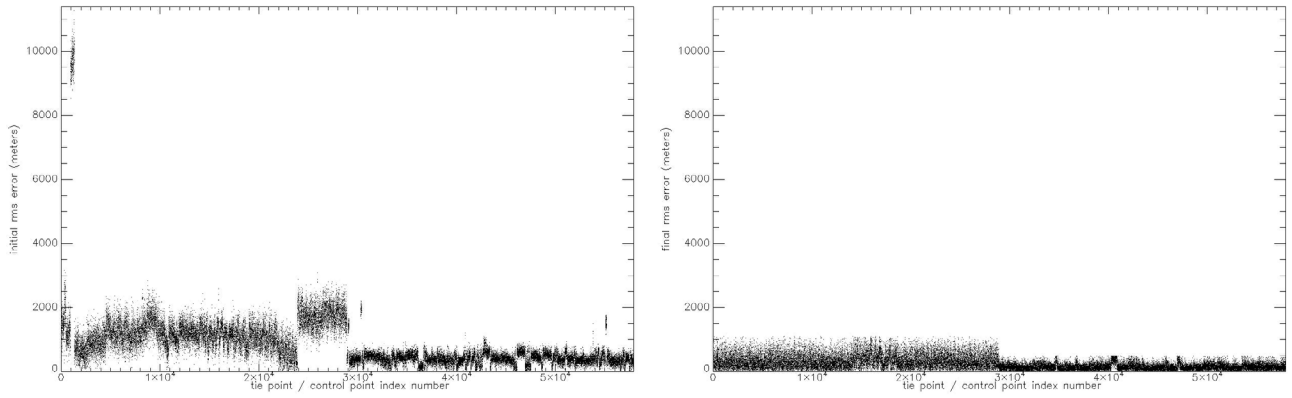

Figure 14. Initial and postoptimization RMS errors for tie points and control points. In each plot the left portion is M^3-to-LOLA control points and the right portion is M^3-to-M^3 tie points. The nominal Global Mode pixel spacing is 140 m for reference. The large and systematic original errors are reduced to being random and much smaller after the attitude-derivation optimization.

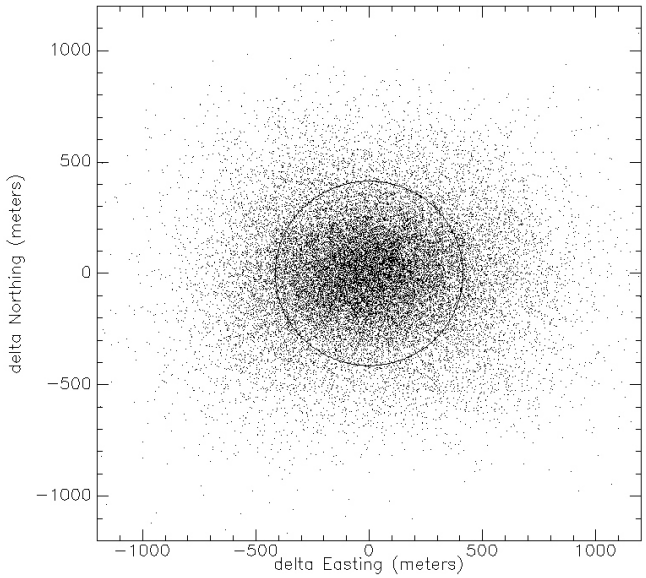

Figure 15. Scatterplot of postoptimization delta easting and delta northing position errors for control points, showing random errors. The nominal Global Mode pixel spacing is 140 m for reference. The circle depicts a radius of 414.3 m, the root-mean-square value for the control point distance residuals.

pseudo control network and the source of our control points. We suspect the larger RMS error in the control point final result is due to the increased challenge of matching M^3 imagery to simulated scenes from illumination of incomplete LOLA topography. This includes the inherent limitations in the LOLA-derived control points where the LOLA coverage was incomplete and interpolated at the kilometer scale. This assertion can be tested when we repeat this process on a future pixel-scale topographic model. Finally, Figure 16 shows the inversion-optimized camera model in the object frame, for comparison to the preflight model shown in Figure 1. Roughly speaking, the M^3 scene-to-scene matching achieved could be considered a measure of the solution precision and the absolute tie to the lunar frame provided by the LOLA control points, in that optimally seamless mosaic, is then a measure of our overall accuracy. However, in a large global model such as ours, where we solve simultaneously for parameters to optimize both control and tie points, precision and accuracy are more tightly linked than a simple consideration might suggest.

[28] Optical Period 1 data were then re-ray-traced using the optimized camera model and the data-derived spacecraft attitude. Since we solved for the combined effect of the variable per orbit spacecraft attitude and the fixed but unknown sensor-to-body angles associated with the alignment of the M^3 boresight, we did not separately break out these two rotational transformations in our model. Our selenolocation results for Optical Period 1 exhibit the desired characteristics of having nearly seamless scene-to-scene mosaicking and are well aligned to the absolute lunar reference frame as expressed by the LOLA data, as indicated by the control point error. Initial processing of data from the 100 km orbit portion of Optical Period 2 shows similar good results. For the 200 km orbit data we have expanded the attitude model to accommodate an initial state, an arbitrary inertial rotation axis and a rotation rate around this axis; this was necessary since the attitude knowledge and control of the spacecraft were degraded during the final months of the mission. This extended model is showing similar quality results for the late-mission data in terms of RMS errors for tie points and control points.

[29] Despite problems with ephemeris, attitude and timing data, we have successfully processed all of the data from Optical Period 1 using the two-tier bootstrapping methodology described here. These selenolocation and observation geometry data are in our initial PDS delivery of the M^3 Level 1B archive in June 2010, and are described in section 6. While processing of a few especially problematic images from Optical Period 2 data is ongoing, the initial Optical Period 2 Level 1B data were delivered to PDS in December 2010. As improved lunar topographic models become available, we will assess whether the M^3 data would benefit

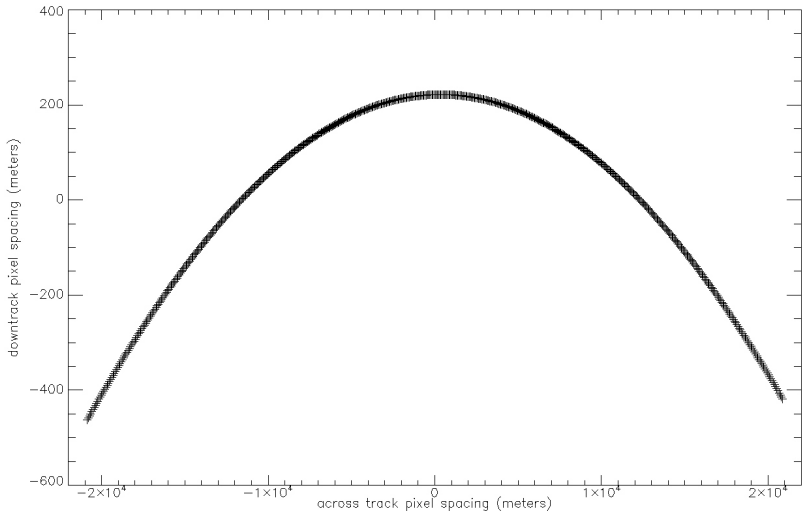

Figure 16. Postinversion camera model depicting nominal pixel-center spacings as projected onto a horizontal surface from an altitude of 100 km.

Table 2. Summary of Chandrayaan-1 Four Flight Modes and Relevant M^3 Sample and Line Flipping and Offsets

Flight mode	Start Time UTC	L0 to L1B Flipping
descending/forward	2008 NOV 16 23:59:59.817219	none
descending/reversed	2008 DEC 18 04:07:59.816462	sample order
ascending/reversed	2009 MAR 15 14:09:59.814432	line order
ascending/forward	2009 JUN 18 01:59:59.815533	both sample and line order

from a complete spatial reprocessing using the improved auxiliary data expected before completion of the contracts of our science team in December 2011.

6. Spatial Products in the M^3 Level 1B Archive

[30] M^3 Level 0 and Level 1B data are archived in the Planetary Data System through the Imaging Node [*Eliason et al.*, 1996]. Optical Period 1 data were delivered in June of 2010 and Optical Period 2 data were delivered in December 2010. Full-mission Level 2 reflectance data will be delivered in June 2011. The spatial processing results, selenolocation and observation geometry, form a portion of the M^3 Level 1B archive. These results are organized as images of derived values, matching the sample and line dimensions of the accompanying radiance files and can be considered "backplanes" for the spectral radiance images. The backplane images contain selenolocation and observation geometry values for each observed spectrum. An additional text file reports the timing of each image frame, derived from our improved clock model. Here we discuss the results of the spatial processing and give examples of the contents of the backplane images. Byte-level details of the data, file formats and the overall archive are given in the M^3 Data Product and Archive Volume Software Interface Specification documents (as part of our PDS Imaging Node archive).

[31] During the mission, there were four image acquisition modes that affected the spatial ordering and appearance of the imagery. These four modes correspond to the four combinations of forward and backward flight (0° and 180° yaw) and lit imaging on descending or ascending limbs of the orbit. Of these four modes, only one is "normal" in terms of having North up and west to the left; as viewed in the canonical image processing coordinate system where sample numbers increase to the right and line numbers increase downward (i.e., pixel 1,1 in the upper left). This "normal" mode is forward flight and lit imaging on the descending limb, which occurred during the initial part of the mission. To make all of the Level 1B radiance data more approachable and uniform, we chose to reverse sample and line ordering, as required in each of the other three modes, to recreate this "normal" layout. All Level 1B images, radiance and spatial product backplanes, have had the required sample and line reordering performed to have north up and west to the left. Table 2 lists the time intervals of the four flight modes during the Chandrayaan-1 mission and the resulting sample and line flips applied to the Level 1 data. Level 0 data are not sample flipped nor line flipped, as they archive the raw data as recorded by the sensor. As such, for all images one must perform sample and line flipping (except those before 18 December 2008) and sample subsetting as outlined in Table 2 to align Level 0 data with Level 1B data.

[32] The selenolocation results from the pixel-by-pixel ray tracing are stored in a three-band LOC file (e.g., M3G20090103T084105_V01_LOC), where the three bands contain the longitude, latitude and radius for the derived center point of each pixel. These values are stored in an 8 byte floating point representation to preserve precision and the file is organized in a band interleaved by line (BIL) format. The number of samples and lines match the

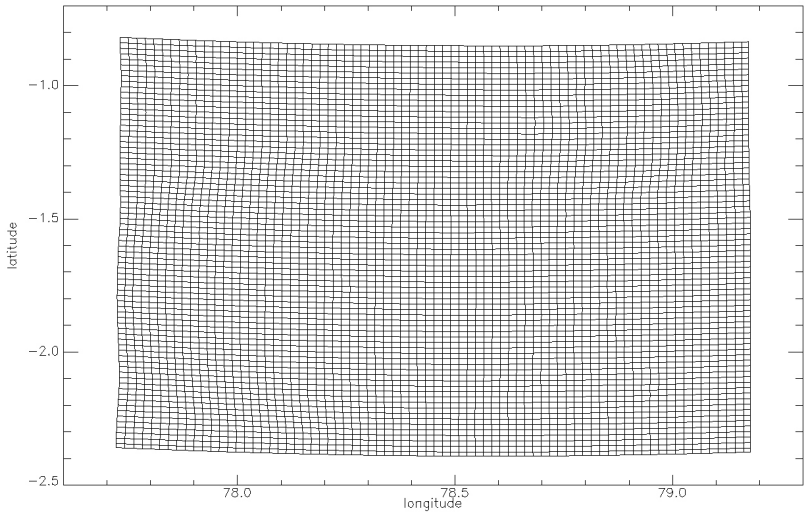

Figure 17. Plot of every fourth row and column of pixel centers in a 300 line subset of a near-equatorial Global Mode scene, showing longitude versus latitude. The curved M^3 slit projection and distortions due to the field of view and topography are apparent.

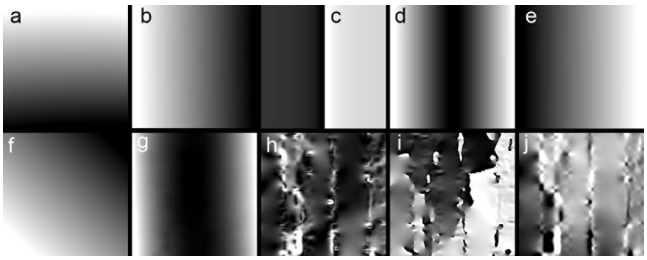

Figure 18. Mosaic of images of the 10 observation geometry values of a 300 line subset of a near-equatorial Global Mode scene. (a) To-Sun azimuth 89.2°–90.7°, (b) to-Sun zenith 45.9°–47.4°, (c) to-M^3 azimuth 2.2°–359.1°, (d) to-M^3 zenith 1.5°–12.8°, and (e) phase angle 34.6°–58.2°. (f) To-Sun path length minus mean of 1.01 AU, (g) to-M^3 path length 111.6–114.3 km, (h) local slope 0.0°–5.4°, (i) local aspect 0°–360°, and (j) local cosine of incidence angle 0.64–0.74 unitless.

accompanying radiance file. The longitude is expressed as degrees east (0–360), and the reference frame is the lunar mean-Earth/polar axis (MOON_ME) frame [*NASA*, 2008]. Figure 17 shows a scatterplot of the longitude and latitude values for all the pixels in a subset of 300 lines of a global image near the equator. The curvature of the M^3 projected slit, the panoramic distortion due to the 24° field of view and the effects of the lunar topography are apparent. The LOC backplane images provide the lunar coordinates for every M^3 pixel. The third band in the LOC file, the lunar radius at each pixel center point, essentially replicates the topographic model as "seen" or sampled by the pixel centers of the M^3 push-broom sampling.

[33] The pertinent facts of the observation and illumination geometry are reported in a ten-band OBS backplane file (e.g., M3G20090103T084105_V01_OBS). Table 3 lists the 10 observation parameters in the OBS files and their associated units. These parameters are stored as 4 byte floating-point representations in band interleaved by line backplane files that match the sample and line dimensions of the accompanying spectral radiance image. The to-Sun and to-M^3 azimuth and zenith angles relative to a local topocentric frame are reported in the first four values. The associated phase, the angle between the to-Sun and to-M^3 vectors, is the fifth value. The sixth and seventh values capture the path lengths from the sun to the pixel center and from the pixel

Table 3. The Observational Geometry Parameters and Their Units as Reported in the OBS Files of the Level 1B M^3 PDS Archive[a]

Observational Parameter	Units
To-Sun Azimuth	Degrees
To-Sun Zenith	Degrees
To-M^3 Azimuth	Degrees
To-M^3 Zenith	Degrees
Phase	Degrees
To-Sun Path Length	Astronomical Units
To-M^3 Path Length	Meters
Local Topography Slope	Degrees
Local Topography Aspect	Degrees
Local Topography Cosine I	Unitless

[a]Slope, aspect, and cosine I are derived from a local LOLA-derived topography model using a 3 × 3 kernel.

Table 4. Subset of an Example Time File

Frame Number	UTC Time	Year	Decimal Day of Year
1	2009-04-23T19:19:45.109303	2009	112.805383228364
2	2009-04-23T19:19:45.007544	2009	112.805382050589
3	2009-04-23T19:19:44.905784	2009	112.805380872814
4	2009-04-23T19:19:44.804024	2009	112.805379695039

center to the sensor. To preserve precision, and allow for 4 byte encoding, we have subtracted the mean to-Sun value for each image file and report it separately in the PDS label for the file as a single scalar for each image. Finally the last three values in the OBS data for a pixel report the local slope, aspect and cosine of the incidence angle, as derived from the topographic model used in the ray tracing and seleno location processing. Figure 18 is a mosaic of images of the 10 backplane value for another 300 line subset of pixels. The incomplete state of the topography model at the time of the processing can be seen in the last three images. Certainly these results show how the M^3 data could benefit from a reprocessing on a pixel-scale topographic model, once available. The slope, aspect and cosine I values reported here are derived from the LOLA topography and in places use average and interpolated values over kilometer scales, and thus are limited in their absolute accuracy and spatial scale. The observation geometry parameters archived in the OBS files provide critical inputs for quantitative processing of the M^3 spectral radiance data. They are required for accurate photometric [*Hicks et al.*, 2010] analysis and for the radio-

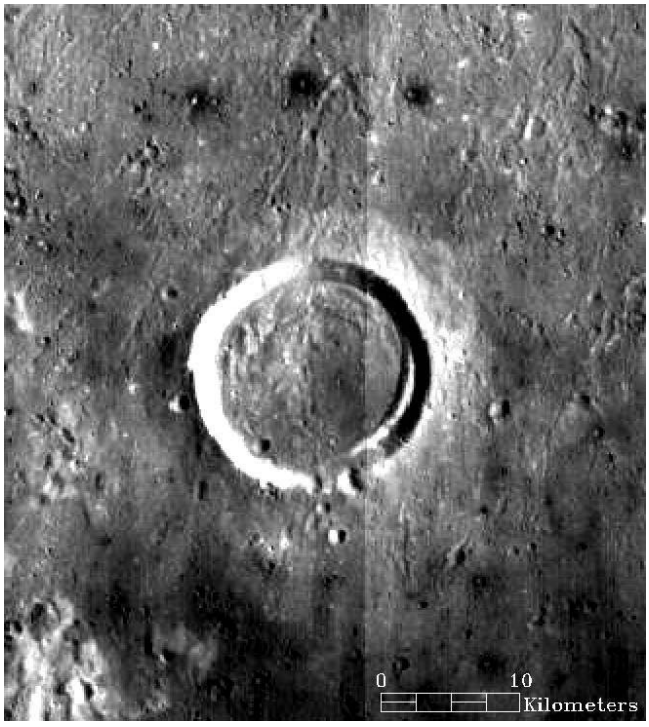

Figure 19. A close-up at full resolution of a single strip-to-strip edge in the M^3 mosaic showing the near-seamless mosaic result achieved, Transverse Mercator projection with 140 m pixels.

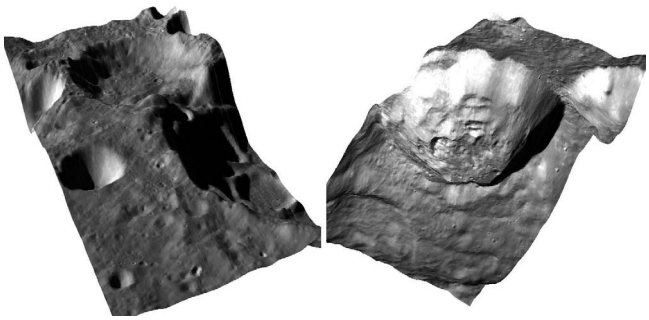

Figure 20. Two 3-D views of M^3 data draped over LOLA topography after ray tracing optimization showing the good match between the LOLA topography and the M^3 imagery, vertical exaggeration of 4X. Subsets of a single swath, 42 km wide, and centered at (left) 62.103°N, 92.529°W and (right) 59.337°N, 92.836°W. Note the alignment of the shadows with the LOLA-derived topography.

metric and thermal processing required to derived surface reflectance [*Clark et al.*, 2010].

[34] The final product of the spatial processing in the Level 1B archive relates to the timing of the observations. A TIM text file is provided for each image file (e.g., M3G20090103T084105_V01_TIM.TAB) that contains one record for each line in the image. The timing data represent the derived midintegration time for each frame of the push-broom image. An example of the three columns of a TIM file are shown in Table 4, reporting line number, UTC time and decimal day of calendar year. The time data in the TIM files have had the appropriate line number reversals applied, where needed, to align with the Level 1B images, as described above.

[35] The results of the spatial processing of the M^3 data are archived as selenolocation (LOC), observation geometry (OBS) and timing (TIM) files in the Level 1B PDS delivery. They, along with the arrived ephemeris, derived attitude, clock and camera model data, contain the fundamental information required for quantitative scientific uses of the data. The format and content of the files has been designed to maximize clarity, utility and information content. Our intent was to provide a Level 1B archive that is user ready and user friendly, yet preserves the details, inherent properties and high fidelity of the imaging spectrometry measurements made by M^3 on Chandrayaan-1.

7. Summary and Conclusions

[36] The Moon Mineralogy Mapper flown on Chandrayaan-1 for an abbreviated 10 month mission exceeded its baseline

Figure 21. A 6039 × 6681 mosaic of 33 M^3 image strips over the Orientale region, demonstrating the stability of the inversion result over large areas. The image-to-image boundaries are still visible in this mosaic of Level 1B radiance, as no photometric corrections have been applied to the over 40 million M^3 spectra in this image. Local Transverse Mercator projection, 140 m pixels.

requirements, covering more than 95% of the Moon in its Global Mode of data acquisition. The mission was hindered by thermal problems with the spacecraft that had implications for the spatial processing and related products of M^3. Notably the attitude data available were incapable of giving a coherent solution, possibly due to the loss of the star sensors during the mission. Nevertheless, we have been able to develop an alternative selenolocation strategy that bootstraps attitude and camera calibration parameters directly from the data, using automatically generated control and tie points. Specifically the very accurate LOLA topographic data and JPL lunar ephemeris allowed us to pursue this bootstrapping approach to the selenolocation process.

[37] Our initial goal was to have M^3-to-M^3 spatial alignment on the scale of the M^3 pixel size (nominally 140 m in Global Mode from 100 km) and we have achieved this despite the numerous operational complications. Figure 19 shows a close-up of a single scene-to-scene boundary. While there are signal level differences, as the mosaic is of radiance images before photometric correction, the spatial alignment is certainly subpixel. Figure 20 shows two subsets of M^3 data draped over LOLA topography after orthorectification. The quality of overall match between the images and the topographic model is, at least, at the several-pixel level and indicative of the resulting accuracy of the solution. This degree of absolute tie to the LOLA frame is reflected in the 414.3 m RMS error for M^3 to LOLA control points. Figure 21 shows a large multiple-orbit mosaic of the Orientale region illustrating the stability and uniformity of the results over a wide area of the Moon.

[38] While we have generally succeeded in our effort to develop the required supporting spatial information for M^3, further work remains. The current results are limited by the incomplete lunar topography model we used and further complicated by the disparate attitude models we developed over the course of our processing during the mission duration. For the M^3 data to be fully exploited they should be re-ray-traced to a global pixel-scale lunar topographic model, once available, and processed in a full-mission sense with a single, robust attitude bootstrapping methodology. Nevertheless, the current spatial products of selenolocation and observation geometry backplanes described here will be valuable for all users of the Moon Mineralogy Mapper data, as they explore this unique data set and its rich information content.

[39] **Acknowledgments.** The authors gratefully acknowledge the heroic efforts of the ISRO Chandrayaan-1 Mission Operations team, notably N. S. Hegde and S. Gomathi. In the face of long odds and rapidly changing situations, the ISRO team saved the spacecraft and our mission. We are deeply indebted to the JPL Navigation Team, especially Neil Mottinger, for the processed ephemeris data and to the LOLA team for access to critical topographic information. We thank NASA SMD and JPL for the Discovery Mission of Opportunity that became the Moon Mineralogy Mapper on Chandrayaan-1. Finally, the lead author expresses his profound thanks to Brent Archinal for his unfailing and patient support, advice, and assistance.

References

Acton, C. H. (1996), Ancillary data services of NASA's Navigation and Ancillary Information Facility, *Planet. Space Sci.*, *44*(1), 65–70, doi:10.1016/0032-0633(95)00107-7.

Araki, H., et al. (2009), Lunar global shape and polar topography derived from Kaguya-LALT laser altimetry, *Science*, *323*(5916), 897–900, doi:10.1126/science.1164146.

Archinal, B. A., M. R. Rosiek, R. L. Kirk, and B. L. Redding (2006), The Unified Lunar Control Network 2005, *U.S. Geol. Surv. Open File Rep.*, *2006-1367*.

Clark, R. N., C. M. Pieters, R. O. Green, J. W. Boardman, and N. E. Petro (2010), Thermal removal from near-infrared imaging spectroscopy data of the Moon, *J. Geophys. Res.*, doi:10.1029/2010JE003751, in press.

Eliason, E. M., S. K. LaVoie, and L. A. Soderblom (1996), The imaging node for the Planetary Data System, *Planet. Space Sci.*, *44*(1), 23–32, doi:10.1016/0032-0633(95)00103-4.

Folkner, W. M., J. G. Williams, and D. H. Boggs (2008), The planetary and lunar ephemeris DE 421, *JPL Memo. 343R-08-003*, Jet Propul. Lab., Pasadena, Calif. [Available at ftp://ssd.jpl.nasa.gov/pub/eph/planets/ioms/de421.iom.v1.pdf.]

Goswami, J. N., and M. Annadurai (2009), Chandrayaan-1: India's first planetary science mission to the moon, *Curr. Sci.*, *96*(4), 486–491.

Green, R. O., et al. (2011), The Moon Mineralogy Mapper (M^3) imaging spectrometer for lunar science: Instrument description, calibration, on-orbit measurements, science data calibration and initial on-orbit validation, *J. Geophys. Res.*, doi:10.1029/2011JE003797, in press.

Hare, T. M., B. A. Archinal, T. L. Becker, E. M. Lee, L. R. Gaddis, B. L. Redding, and M. R. Rosiek (2008), Clementine mosaics warped to ULCN 2005 network, *Lunar Planet. Sci.*, *XXXIX*, Abstract 1092.

Haruyama, J., M. Ohtake, T. Matsunaga, T. Morota, C. Honda, Y. Yokota, and Y. Ogawa (2009), Selene (Kaguya) terrain camera observation results of nominal mission period, *Lunar Planet. Sci.*, *XL*, Abstract 1553.

Hicks, M. D., B. J. Buratti, J. Nettles, M. Staid, C. M. Pieters, S. Bess, and J. Boardman (2010), A photometric function for analysis of lunar images in the visual and infrared based on Moon Mineralogy Mapper observations, *J. Geophys. Res.*, doi:10.1029/2010JE003733, in press.

Jet Propulsion Laboratory (2010), Planetary Data System archive preparation guide, version 1.4, *Rep. JPL D-31224*, Pasadena, Calif. [Available at http://pds.nasa.gov/documents/apg/apg.pdf.]

Levenberg, K. (1944), A method for the solution of certain non-linear problems in least squares, *Q. Appl. Math.*, *2*, 164–168.

Lowe, D. G. (2004), Distinctive image features from scale-invariant keypoints, *Int. J. Comput. Vis.*, *60*(2), 91–110, doi:10.1023/B:VISI.0000029664.99615.94.

Marquardt, D. (1963), An algorithm for least-squares estimation of nonlinear parameters, *SIAM J. Appl. Math.*, *11*, 431–441, doi:10.1137/0111030.

Mouroulis, P., R. O. Green, and T. G. Chrien (2000), Design of pushbroom imaging spectrometers for optimum recovery of spectroscopic and spatial information, *Appl. Opt.*, *39*(13), 2210–2220, doi:10.1364/AO.39.002210.

NASA (2008), A standardized lunar coordinate system for the Lunar Reconnaissance Orbiter and lunar datasets, *LRO Proj. LGCWG White Pap.*, *5*, Goddard Space Flight Cent., Greenbelt, Md. [Available at http://lunar.gsfc.nasa.gov/library/LunCoordWhitePaper-10-08.pdf.]

Robinson, M. S., S. M. Brylow, M. Tschimmel, D. Humm, S. J. Lawrence, P. C. Thomas, B. W. Denevi, E. Bowman-Cisneros, J. Zerr, and M. A. Ravine (2010), Lunar Reconnaissance Orbiter Camera (LROC) instrument overview, *Space Sci. Rev.*, *150*, 81–124, doi:10.1007/s11214-010-9634-2.

Smith, D. E., et al. (2010), Initial observations from the Lunar Orbiter Laser Altimeter (LOLA), *Geophys. Res. Lett.*, *37*, L18204, doi:10.1029/2010GL043751.

S. Besse, Department of Astronomy, University of Maryland, Computer Space Science Bldg., College Park, MD 20742, USA.

J. W. Boardman, Analytical Imaging and Geophysics, LLC, 4450 Arapahoe Ave., Ste. 100, Boulder, CO 80305, USA. (boardman@aigllc.com)

R. O. Green, S. R. Lundeen, and P. Varanasi, Jet Propulsion Laboratory, 4800 Oak Grove Dr., M. S. 306-438, Pasadena, CA 91109, USA.

P. Isaacson, J. Nettles, and C. M. Pieters, Department of Geological Sciences, Brown University, Providence, RI 02912, USA.

N. Petro, NASA Goddard Space Flight Center, Mail Code 698, Greenbelt, MD 20771, USA.

L. A. Taylor, Planetary Geosciences Institute, University of Tennessee, Knoxville, TN 37996, USA.